remote sensing

MDPI

Article

Compatible Biomass Model with Measurement Error Using Airborne LiDAR Data

Xingjing Chen [1,2], Dongbo Xie [1,2], Zhuang Zhang [1,2], Ram P. Sharma [3], Qiao Chen [1,2], Qingwang Liu [1] and Liyong Fu [1,2,*]

[1] Research Institute of Forest Resource Information Techniques, Chinese Academy of Forestry, Beijing 100091, China; chenxj@ifrit.ac.cn (X.C.); xiedongbo@caf.ac.cn (D.X.); zhangz@cfgc.cn (Z.Z.); chenq@ifrit.ac.cn (Q.C.); liuqw@ifrit.ac.cn (Q.L.)
[2] Key Laboratory of Forest Management and Growth Modeling, National Forestry and Grassland Administration, Beijing 100091, China
[3] Institute of Forestry, Tribhuwan Univeristy, Kritipur 44600, Nepal; ramsharm1@gmail.com
* Correspondence: fuly@ifrit.ac.cn; Tel.: +86-10-6288-9126

Abstract: Research on the inversion of forest aboveground biomass based on airborne light detection and ranging (LiDAR) data focuses on finding the relationship between the two, such as established linear or nonlinear models. However, these models may have poorer estimation accuracy for tree-components biomass and cannot guarantee the additivity of each component. Therefore, we aimed to develop an error-in-variable biomass model system that ensures both the compatibility of the individual tree component biomass with the diameter at breast height and the additivity of component biomass. The system we developed used the airborne LiDAR data and field-measured data of principis-rupprechtii (*Larix gmelinii* var.) trees, collected from north China. Our model system not only ensured the additivity of nonlinear biomass models, it also accounted for the impact of measurement errors. We first selected the airborne LiDAR-derived variable with the highest contribution to the biomass of each component and then developed an inversion model system with that variable as an independent variable and with the biomass of each component as the dependent variable using allometric functions. Moreover, two model estimation methods, two-stage error (TSEM) and nonlinear seemingly unrelated regression (NSUR) with one-step, two-step, and summation methods, were also applied, and their performances were compared. The results showed that both NSUR-one-step and TSEM-one-step led to similar parameter estimates and performance for a system, and the fitting accuracy of a model system was not very attractive. The variance function included in a model system reduced the heteroscedasticity effectively and improved the model accuracy. Overall, this study successfully combined the error-in-variable modeling with the airborne LiDAR data, proposed methods that can be used for the extension of component biomass from an individual tree to a stand and that might improve the estimation accuracy of carbon storage. A compatible model system can be further improved if various sources of error in the variables are identified, and their impacts on the system are effectively accounted for.

Keywords: airborne LiDAR; tree-components biomass; error-in-variable model; nonlinear seemingly unrelated regression

Citation: Chen, X.; Xie, D.; Zhang, Z.; Sharma, R.P.; Chen, Q.; Liu, Q.; Fu, L. Compatible Biomass Model with Measurement Error Using Airborne LiDAR Data. *Remote Sens.* **2023**, *15*, 3546. https://doi.org/10.3390/rs15143546

Academic Editor: Luis A. Ruiz

Received: 30 May 2023
Revised: 1 July 2023
Accepted: 11 July 2023
Published: 14 July 2023

1. Introduction

As a basis of estimating forest carbon storage and evaluating the contribution to the forest carbon cycle, forest biomass plays an important role in forest ecosystems, and aboveground biomass (AGB) accounts for a large proportion of it [1]. Therefore, the accurate quantification of forest AGB is of great significance to forest managers. Accurate biomass measurement requires the cutting down of individual trees and drying and weighting them. However, this is not practically feasible for a large forest area. Alternatively, developing allometric biomass equations using the diameters at breast height (DBH) and tree height

(H) of some representative sample trees as independent variables is another method. Many studies have also proved that DBH used as the predictor in the tree biomass model performed adequately well [2,3]. Allometric equations are also used to estimate the biomasses of different tree components (henceforth tree-components). Different tree-components are widely used. For example, bark can be used as a soil conditioner [4,5], and foliage plays an important role in protecting soil from water erosion and maintaining biodiversity [6,7]. Thus, quickly and easily estimating tree-component biomass is also an important part of forest management. However, it can be time-consuming and costly while destructively measuring tree variables in a large forest area.

Light detection and ranging (LiDAR) technology has been applied to forestry research since the mid-1980s. Previous studies found that the LiDAR system can estimate tree height [8,9]. MacLean and Krabill [10] found that tree canopy volume could be estimated using the laser radar reconstruction of the canopy profile. Subsequently, many studies demonstrated that the LiDAR system could accurately estimate forest parameters, such as basal area, stock volume, and biomass [11–15]. For instance, the estimation of biomass using LiDAR is primarily divided into two aspects: plot-level and individual-tree level. The plot-level estimation is achieved by establishing mathematical relationships between LiDAR variables and the biomass, with an emphasis on model forms and parameter estimation methods [16–19]. The individual-tree level requires accurate segmentation of individual trees from LiDAR data in order to model and estimate the biomass of specific components or the entire tree [14,20]. Therefore, the acquisition of inventory factors by remote sensing techniques gradually matured [20–24].

Nonlinear least square regression (NLS) is a common method for estimating parameters of the allometric equations, such as tree growth equations [20,25,26]. NLS has a number of assumptions while modeling, and a violation of any assumption leads to the biased estimates of the parameters [27,28]. To deal with this problem, estimation of the NLS equation needs to be estimated using the seemingly uncorrelated regression (SUR) method [29–34]. Previous methods of estimating tree biomass include: (1) only stem is considered for construction with one equation, which results in the univariate model and binary model; and (2) all the tree-components are considered for a model system construction using different models. The former method is not complete, and the latter method has a remarkable drawback, such as low accuracy, because of different responses to the factors for different tree-components. Different tree-component biomass models are constructed independently, which leads to the ignorance of the correlation between the components [35]. To solve the additivity problems, additive biomass equations can be developed [34,36,37].

Similarly, tree biomass estimation based on LiDAR data has the same problems, as pointed out above. The independent variables in a biomass equation should be free of measurement errors, which is a prerequisite for the use of the nonlinear seemingly uncorrelated regression (NSUR) simultaneous equations. However, the independent variables, such as DBH, H, crown width, etc., can be derived from remote sensing products and used for data processing and analysis and may contain substantial random errors and systematic errors [38,39]. The potential solution to these problems is to develop LiDAR-based biomass models using error-in-variable modeling, which ensures the additivity of tree-component biomass models while taking measurement errors into account [25,27,39–41]. However, only a few of the existing biomass modeling studies have considered the additivity of biomass equations and have failed to recognize the inherent correlation between the tree-component biomass and DBH.

Therefore, we developed the error-in-variable biomass models for predicting forest aboveground biomass based on airborne LiDAR data, with the aim of ensuring the compatibility of the individual tree component biomass with DBH and the additivity of components when estimating biomass. The main elements of this study were as follows: (i) The error-in-variable modeling approach was used to develop a system of compatible AGB and individual tree-components biomass with airborne LiDAR data; and (ii) NSUR was applied as the parameter estimation method. This study can be novel, as it considers

the measurement errors and ensures the additivity of tree-components biomass on the airborne LiDAR data. This method may be applied for a large-scale biomass prediction purpose (from individual to stand), and the model-considering the additivity of each component would accurately estimate stand biomass.

2. Materials and Methods

In Figure 1, we present a flowchart of the developed, compatible individual tree DBH and the tree-components biomass model system using airborne LiDAR data. The main steps included: (1) acquisition of LiDAR data and field-measured data; (2) derivation of LiDAR-based variables for individual trees; (3) development of the LiDAR-DBH model and LiDAR-tree-components model; (4) construction of the biomass model prediction system through three model forms (one-step, two-step, and summation) and two parameter estimation methods (TSEM and NSUR); and (5) elimination of model heteroscedasticity using weighting functions.

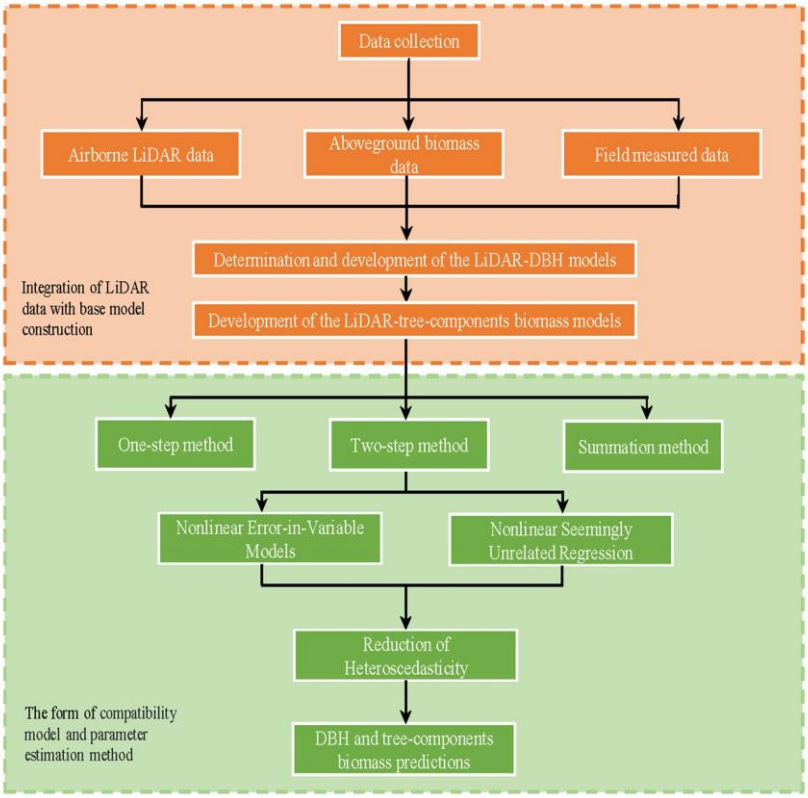

Figure 1. The flowchart of the developed, compatible individual tree diameter at breast height (DBH) and tree-components biomass model system using airborne LiDAR data.

2.1. Study Area

The study area was located at the 2022 Winter Olympics Core of Chongli County, Hebei Province, China (Figure 2). The area covered about 20 sq. km, and the average altitude was 1400 m. The forest of this area was dominated by *Larix gmelinii* var. principis-rupprechtii and *Betula platyphylla Suk.*, where *Larix gmelinii* var. principis-rupprechtii was artificial forest, and *Betula platyphylla Suk.* was natural forest.

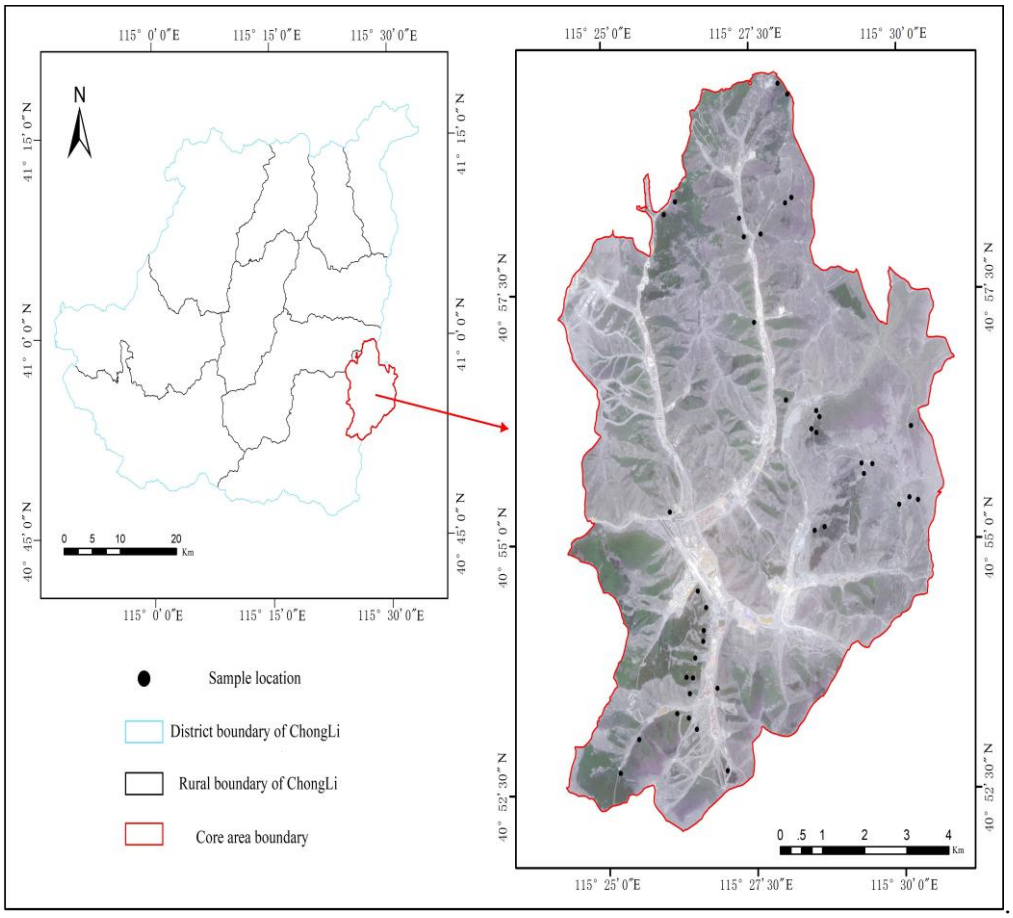

Figure 2. Location of the study area: the 40 permanent sample plots of 30 m × 30 m (CGCS2000 3-degree Gauss Kruger CM 114E) established in the 2022 Winter Olympics Core of Chongli County, Hebei Province, China.

2.2. Data Collection

2.2.1. Field Data Collection

Forty permanent sample plots were established in the pure *Larix gmelinii* var. principis-rupprechtii forest covering the entire age class in August 2021. For each sample plot, all trees with DBH > 2 cm were measured for DBH. The coordinates of the four corners of the sample plot and the positions of the trees were measured using RTK (real-time kinematic) to improve the accuracy of the sample plot establishment and the convenience of repetitive measurements. The distribution of the sample plots and the statistical analysis of measured data are presented in Figure 2 and Table 1, respectively.

2.2.2. Airborne LiDAR Data Acquisition

Airborne LiDAR data were acquired simultaneously with field survey works using a multi-rotor UAV equipped with an AS-1300HL laser radar measurement system. The laser scanner was GL-52, with a wavelength of 780~3000 nm. The celestial angle was −33°~33°, and the pulse emission frequency was 600 kHz. The mean flight speed was 6 m s^{-1}, the mean flight height was 150 m, the point cloud side overlap rate was 50%, and the mean density was 46 pts m^{-2}. The LiDAR carried an orthographic camera during flight to take an orthographic image of the flight area, which allowed the researchers to visualize the study area (Figure 3).

Table 1. Summary statistics of individual tree variables (W_P , protoxylem biomass; W_B, branch biomass; W_{BK}, bark biomass; W_F, foliage biomass; W_{AG}, aboveground biomass; W_S, stem biomass; W_C, crown biomass; LH, LiDAR-derived tree height; DBH, field-measured diameter at breast height; CD, crown diameter; CPA, crown projection area; and SD, standard deviation).

Variable	Min	Mean	Max	SD
W_P (kg)	0.24	42.51	164.08	29.76
W_B (kg)	0.22	16.5	53.5	10.1
W_{BK} (kg)	0.12	8.11	25.53	4.85
W_F (kg)	0.17	4.82	12.59	2.44
W_S (kg)	0.37	50.62	189.61	34.59
W_C (kg)	0.38	21.32	66.09	12.53
W_{AG} (kg)	0.75	71.94	55.70	47.09
LH (m)	1.05	9.68	17.27	3.07
DBH (cm)	2.1	15.76	29.4	5.40
CD (m)	0.79	2.69	5.52	0.8
CPA (m^2)	0.35	6.17	24	3.66

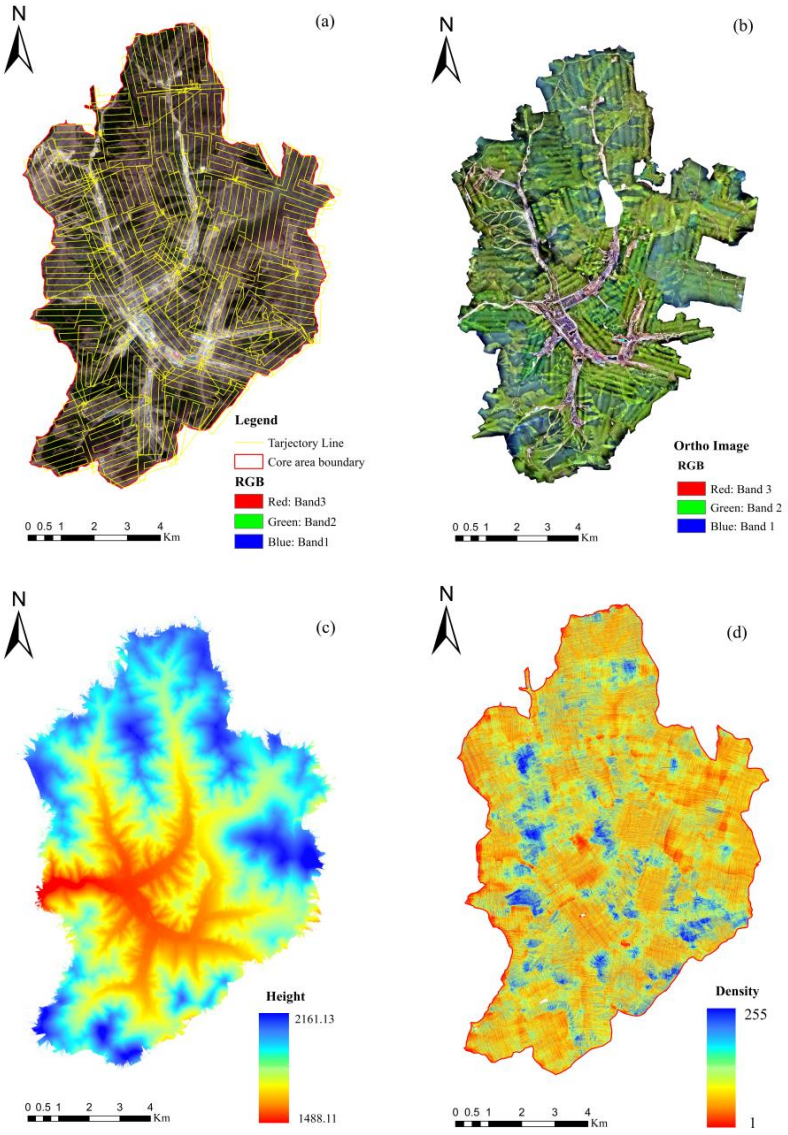

Figure 3. Four images of the study area (CGCS2000 3-degree Gauss–Kruger CM 114E); (**a**) the Trajectory line with airborne LiDAR; (**b**) the ortho image with airborne LiDAR; (**c**) the spatial distribution of elevation (m ASL—above sea level); (**d**) the density of the laser points (points per m^2).

2.2.3. LiDAR-Based Extraction of Individual Tree Characteristics

Similar to most LiDAR inversion studies [42,43], the canopy height model was obtained by subtracting the digital elevation model from the digital surface model to further extract individual tree information. The first mainstream individual tree crown delineation method was known as the 'watershed method' [44], and another mainstream method was segmenting the LiDAR point into polygons based on the tree crown edges and considering the maximum value in the polygon as the top of the crown. Although previous studies indicated that tree crown-related factors, such as asymmetric crown shape, tree overlap, and short tree crowns, could result in the under-segmentation of individual tree crowns, the impact was less pronounced for conifer tree species with distinct tree tops [45]. Additionally, the resolution of raster data played a dominant role in segmentation accuracy [20]. Furthermore, several studies showed that the first method could obtain more accurate results of tree crown segmentation, and therefore, we applied this method [46].

The LiDAR point cloud data processing involved: (1) classifying ground LiDAR points to obtain the digital elevation model and carrying out the normalization process; (2) obtaining the digital surface model, which applied the maximum height interpolation method [46]; and (3) obtaining individual tree information by using the canopy height model, including LiDAR-derived tree height (LH), crown diameter (CD), and crown projection area (CPA). The digital elevation model, digital surface model, and canopy height model had a resolution of 0.5 m $\times$ 0.5 m. To ensure the canopy was not under-segmented, the Gaussian smoothing filter was used with a sigma value of 0.5.

A total of 947 individual principis-rupprechtii tree crowns were delineated based on the above method. Generally, forest biomass modeling and the application of the model needs field measurements, which not only demands more time and more financial resources but also causes a destruction of forests. The forest biomass models based on remote sensing data are often constructed without the destruction of forests. Application of this method could have a high accuracy in forest biomass prediction [47]. We used the empirical allometric models developed by Fu et al. [48] to estimate the biomasses of 947 individual trees, which contained protoxylem, branch, foliage, bark, and aboveground biomass (Table 2). Such a study adopted the allometric biomass equation, with DBH as a single independent variable; the variables of individual trees are summarized in Table 1.

Table 2. Empirical models of tree biomass in north China (Fu et al. [48]).

Biomass	Model
Protoxylem	$W_P = 0.0388\text{DBH}^{2.4696}$
Branch	$W_B = 0.0462\text{DBH}^{2.0865}$
Bark	$W_{BK} = 0.0274\text{DBH}^{2.0222}$
Foliage	$W_F = 0.0496\text{DBH}^{1.6375}$
Stem	$W_S = 0.0618\text{DBH}^{2.3723}$
Crown	$W_C = 0.0837\text{DBH}^{1.9946}$
Above-ground	$W_{AG} = 0.1431\text{DBH}^{2.2193}$

2.3. Method

2.3.1. Variables Selection and Determination of the LiDAR-DBH Base Model

Considering problems such as over-parameterization and collinearity of the model, only those variables that contribute significantly to the variation in DBH were selected in our modeling. We used correlation statistics and graphical analyses to select the variables. We also examined the impacts of variable transformations on biomass models, such as logarithmic transformations. We found that LH contributed significantly highly to the improvement in predictions of DBH.

Five common model forms were used to develop the base model of DBH, with the only predictor variable being the LiDAR-derived tree height. Version 4.1 of R software was

used to estimate models with the NLS technique nls (nonlinear least squares) function [49]. The following statistical criteria were used to evaluate the base model [50]:

$$R^2 = 1 - \sum\left(DBH_i - D\hat{B}H_i\right)^2 / \sum\left(DBH_i - \overline{DBH}\right)^2 \quad (1)$$

$$\bar{\varepsilon} = \sum \varepsilon_i / N = \sum\left(DBH_i - D\hat{B}H_i\right) / N \quad (2)$$

$$\mathrm{TRE} = 100\frac{\sum\left(\mathrm{DBH}_i - D\hat{B}H_i\right)}{\sum D\hat{B}H_i} \quad (3)$$

$$\mathrm{RMSE} = \sqrt{\bar{\varepsilon}^2 + \sigma^2} \quad (4)$$

where DBH_i and $D\hat{B}H_i$ are the observed and predicted DBHs for the ith observation ($i = 1, \ldots, N$), N is the total number of samples, $\overline{DBH}$ is the mean of the DBH observations, $\bar{\varepsilon}$ is the mean bias, R^2 is the coefficient of determination, TRE is the total relative error, σ^2 is the bias variance, and RMSE is the root mean square error.

In this study, LiDAR-derived tree height largely contributed to the tree-components biomass models. Therefore, based on the evaluation of fitted basic models using the statistical criteria mentioned above (Equations (1)–(4), the best performing model was selected for further analysis. The models of biomass and DBH of different components based on the allometric models were established (to be shown later).

2.3.2. Developing Form of a Model System

The error-in-variable model could significantly reduce the problem of the dependent variables containing errors, including measurement errors [51,52]. The general form of such a model is:

$$\begin{cases} f(y_i, x_i, \beta) = 0 & i = 1, \ldots, N \\ Y_i = y_i + e_i & \\ E(e_i) = 0 & \mathrm{Var}(e_i) = \sum \end{cases} \quad (5)$$

where N is the number of samples to construct the model; $f(y_i, x_i, \beta)$ represents the model form; x_i and y_i represent the independent variable and the dependent variables, where the independent variable is without measurement error, and the dependent variable is with measurement error; and $\sum$ is the positive definite variance–covariance matrix of an error term e_i.

We termed sub-models for LiDAR-DBH and AGB models (Table 2). On the basis of model (5), sub-models were developed into a system to ensure the additivity of the model. Additionally, model (5) was developed in 3 forms. The first method divided the aboveground biomass into tree protoxylem, tree branch, tree foliage, and tree bark, and we termed this method the one-step method. It can be expressed as:

$$\begin{cases} w_{1i} = \dfrac{f_1\left(y_i^{(1)}, x_i, \beta_1\right)}{f_1\left(y_i^{(1)}, x_i, \beta_1\right) + f_2\left(y_i^{(1)}, x_i, \beta_2\right) + f_3\left(y_i^{(1)}, x_i, \beta_3\right) + f_4\left(y_i^{(1)}, x_i, \beta_4\right)} \hat{W}_{0i} \\ w_{2i} = \dfrac{f_2\left(y_i^{(1)}, x_i, \beta_2\right)}{f_1\left(y_i^{(1)}, x_i, \beta_1\right) + f_2\left(y_i^{(1)}, x_i, \beta_2\right) + f_3\left(y_i^{(1)}, x_i, \beta_3\right) + f_4\left(y_i^{(1)}, x_i, \beta_4\right)} \hat{W}_{0i} \\ w_{3i} = \dfrac{f_3\left(y_i^{(1)}, x_i, \beta_3\right)}{f_1\left(y_i^{(1)}, x_i, \beta_1\right) + f_2\left(y_i^{(1)}, x_i, \beta_2\right) + f_3\left(y_i^{(1)}, x_i, \beta_3\right) + f_4\left(y_i^{(1)}, x_i, \beta_4\right)} \hat{W}_{0i} \\ w_{4i} = \dfrac{f_4\left(y_i^{(1)}, x_i, \beta_4\right)}{f_1\left(y_i^{(1)}, x_i, \beta_1\right) + f_2\left(y_i^{(1)}, x_i, \beta_2\right) + f_3\left(y_i^{(1)}, x_i, \beta_3\right) + f_4\left(y_i^{(1)}, x_i, \beta_4\right)} \hat{W}_{0i} \\ Y_i = y_i + e_i, Y_i = \left(W_{1i}, W_{2i}, W_{3i}, W_{4i}(Y_i)^T\right)^T, y_i = \left(w_{1i}, w_{2i}, w_{3i}, w_{4i}, \left(y_i^{(1)}\right)^T\right)^T \\ E(e_i) = 0, \mathrm{var}(e_i) = \sigma^2\psi, i = 1, \ldots, N \end{cases} \quad (6)$$

where $i = 1, \ldots, N$, $W_{0i} \sim W_{4i}$ represent the observed biomass values of the aboveground biomass, tree protoxylem, tree branch, tree foliage, and tree bark of the ith tree, with their values containing measurement errors; and the equation function for tree-components are represented by $f_1\left(y_i^{(1)}, x_i, \beta_1\right)$ to $f_4\left(y_i^{(1)}, x_i, \beta_4\right)$. $w_{1i} \sim w_{4i}$ and $\hat{W}_{oi}$ are the measured values.

The structural matrix ψ explains the internal correlation between the tree-components of an individual tree [53].

The second method divided the aboveground biomass into the tree stem and the tree crown, the crown into the tree branch and tree foliage, and the stem into tree protoxylem and tree bark. We termed this method the two-step method. This ensured that tree crown = tree branch + tree foliage, and tree stem = tree protoxylem + tree bark. Its expression was as follows:

$$\begin{cases} w_{1i} = \dfrac{f_1\left(y_i^{(1)},x_i,\beta_1\right)}{f_1\left(y_i^{(1)},x_i,\beta_1\right)+f_3\left(y_i^{(1)},x_i,\beta_3\right)} \dfrac{f_5\left(y_i^{(1)},x_i,\beta_1\right)}{f_5\left(y_i^{(1)},x_i,\beta_1\right)+f_6\left(y_i^{(1)},x_i,\beta_3\right)} \hat{W}_{0i} \\ w_{2i} = \dfrac{f_2\left(y_i^{(1)},x_i,\beta_2\right)}{f_2\left(y_i^{(1)},x_i,\beta_2\right)+f_4\left(y_i^{(1)},x_i,\beta_4\right)} \dfrac{f_6\left(y_i^{(1)},x_i,\beta_1\right)}{f_5\left(y_i^{(1)},x_i,\beta_1\right)+f_6\left(y_i^{(1)},x_i,\beta_3\right)} \hat{W}_{0i} \\ w_{3i} = \dfrac{f_3\left(y_i^{(1)},x_i,\beta_3\right)}{f_1\left(y_i^{(1)},x_i,\beta_1\right)+f_3\left(y_i^{(1)},x_i,\beta_4\right)} \dfrac{f_5\left(y_i^{(1)},x_i,\beta_1\right)}{f_5\left(y_i^{(1)},x_i,\beta_1\right)+f_6\left(y_i^{(1)},x_i,\beta_3\right)} \hat{W}_{0i} \\ w_{4i} = \dfrac{f_4\left(y_i^{(1)},x_i,\beta_4\right)}{f_2\left(y_i^{(1)},x_i,\beta_2\right)+f_4\left(y_i^{(1)},x_i,\beta_4\right)} \dfrac{f_6\left(y_i^{(1)},x_i,\beta_1\right)}{f_5\left(y_i^{(1)},x_i,\beta_1\right)+f_6\left(y_i^{(1)},x_i,\beta_3\right)} \hat{W}_{0i} \\ Y_i = y_i + e_i, Y_i = \left(W_{1i}, W_{2i}, W_{3i}, W_{4i}(Y_i)^T\right)^T, y_i = \left(w_{1i}, w_{2i}, w_{3i}, w_{4i}, \left(y_i^{(1)}\right)^T\right)^T \\ E(e_i) = 0, \mathrm{var}(e_i) = \sigma^2\psi, i = 1, \ldots, N \end{cases} \quad (7)$$

where $f_5\left(y_i^{(1)}, x_i, \beta_1\right)$ and $f_6\left(y_i^{(1)}, x_i, \beta_1\right)$ are the equations corresponding to the tree stem and crown, and the meanings of the other variables are the same as in Equation (6).

The one-step and two-step methods were based on the biomass model of the proportion method (Equations (6) and (7), respectively). The third method was based on the biomass model of the summation method (Equation (8)).

$$\begin{cases} w_{0i} = f_1\left(y_i^{(1)}, x_i, \beta_1\right) + f_2\left(y_i^{(1)}, x_i, \beta_2\right) + f_3\left(y_i^{(1)}, x_i, \beta_3\right) + f_4\left(y_i^{(1)}, x_i, \beta_4\right) + \zeta_{0i} \\ w_{1i} = f_1\left(y_i^{(1)}, x_i, \beta_1\right) + \zeta_{1i} \\ w_{2i} = f_2\left(y_i^{(1)}, x_i, \beta_2\right) + \zeta_{2i} \\ w_{3i} = f_3\left(y_i^{(1)}, x_i, \beta_3\right) + \zeta_{3i} \\ w_{4i} = f_3\left(y_i^{(1)}, x_i, \beta_4\right) + \zeta_{4i} \end{cases} \quad (8)$$

where $\zeta_{0i}, \zeta_{1i}, \zeta_{2i}, \zeta_{3i}$, and ζ_{4i} represent the aboveground biomass and the residuals of protoxylem, branch, foliage, and bark, respectively, and the meanings of the other variables are the same as in Equation (6).

2.3.3. Nonlinear Error-in-Variable Models (NEIVM) and Nonlinear Seemingly Unrelated Regression (NSUR)

The form of the NEIVM was proposed by Fuller [41]. Tang et al. developed this model and divided the variables into two categories, based on whether the variables included measurement errors: error-in-variables and error-out-variables [54]. In this study, the models (6) and (7) were estimated by the two-stage error (TSEM) algorithm in Forstat 3.0 [55]. We selected the biomasses of different components as error variables, with LH as the true value. The specific estimation processes can be found in Tang 2001 [54].

The NSUR is also a common algorithm used to estimate the measurement error model, which uses a feasible generalized least square regression [31,55]. We used NSUR to estimate

the biomass model of the proportion method (Equation (7)) and the summation method (Equation (8)).

There still existed a controversial issue of whether the sample needed to be divided into modeling data and test data [56,57]. Beak and Shao argued that it was unconvincing to evaluate the model only by the indices obtained from the modeling data [58,59]; Weisheng Zeng (1999) also believed that it was not advisable to collect a single set of the test samples for adaptability testing, and all the samples should be used to build the model [60]. To make full use of the sampled data, this study did not distinguish between modeling samples and testing samples.

2.3.4. Heteroscedasticity

For nonlinear joint estimation of biomass models, elimination of the heteroscedasticity was an indispensable step. The common way to eliminate heteroscedasticity is to use the weighted regression method. We used $1/\sqrt[3]{f_i(y_i^{(1)}, x_i, \beta_1)}$, $1/\sqrt{f_i(y_i^{(1)}, x_i, \beta_1)}$, $1/f_i(y_i^{(1)}, x_i, \beta_1)$ and $1/f_i(y_i^{(1)}, x_i, \beta_1)^2$ as weight functions.

3. Results

3.1. LiDAR-DBH Models

Table 3 shows the fitting results for models I.1 to I.5. In contrast, model I.3 and I.4 were slightly better than others (larger R^2), although the differences in fit statistics between the five models were not significant. We also chose model I.4 as the basic nonlinear model because model I.4 was simpler than model I.3.

Table 3. Evaluation statistics for five candidate base models (RMSE, root mean square error; R^2, coefficient of determination; $\bar{\varepsilon}_{DBH}$, mean prediction error; TRE, total relative error; $\alpha_1 - \alpha_3$, model parameters; and ε_{DBH}, error term).

Model	Model	Model Form	RMSE	R^2	$\bar{\varepsilon}_{DBH}$	TRE
I.1	$DBH = \alpha_1 + \alpha_2 LH + \varepsilon_{DBH}$	Linear	4.0462	0.51626	0.00000	6.0526
I.2	$DBH = \alpha_1 LH^{\beta_1} + \varepsilon_{DBH}$	Empirical	4.0276	0.52072	−0.01672	5.9935
I.3	$DBH = \alpha_1/[1 + \alpha_2 \exp(-\alpha_3 LH)] + \varepsilon_{DBH}$	Logistic	4.0127	0.52439	−0.005258	5.9469
I.4	$DBH = \alpha_1[1 - \exp(-\alpha_2 LH)] + \varepsilon_{DBH}$	Richards	4.0154	0.52362	−0.01672	5.9551
I.5	$DBH = \alpha_1 \exp(-\alpha_2 LH) + \varepsilon_{DBH}$	Exponential	4.1903	0.48120	−0.04616	6.5199

Table 4 shows the models of biomass and DBH of different components, based on the allometric models. The stem biomass was summed by the protoxylem and bark, the crown biomass was summed by the branch and foliage, and the aboveground biomass was summed by the protoxylem, branch, bark, and foliage.

Table 4. Seven different tree-component base models of biomass estimation and their evaluation statistics ($\bar{\varepsilon}_W$, mean prediction error; $\beta_1 - \beta_3$, model parameters; and ε_W, error term).

Model	Model	Components	RMSE	R^2	$\bar{\varepsilon}_W$	TRE
II.1	$W_P = \beta_1 DBH^{\beta_2} + \varepsilon_W$	Protoxylem	8.6527	0.5900	−0.0717	11.8530
II.2	$W_B = \beta_3 DBH^{\beta_4} + \varepsilon_W$	Branch	22.7314	0.5657	−0.1633	15.8248
II.3	$W_{BK} = \beta_5 DBH^{\beta_6} + \varepsilon_W$	Bark	3.1095	0.5882	−0.0257	12.1274
II.4	$W_F = \beta_7 DBH^{\beta_8} + \varepsilon_W$	Foliage	6.5137	0.5839	−0.0534	12.7763
II.5	$W_{AG} = \beta_9 DBH^{\beta_{10}} + \varepsilon_W$	Aboveground	31.5338	0.5753	−0.2478	14.1597
II.6	$W_S = \beta_{11} DBH^{\beta_{12}} + \varepsilon_W$	Stem	19.7480	0.5598	−0.1305	16.9231
II.7	$W_C = \beta_{13} DBH^{\beta_{14}} + \varepsilon_W$	Crown	1.5162	0.6143	−0.0114	8.5341

3.2. Model Parameter Estimates

Table 5 lists the parameter estimates of the models fitted by NEIVM and NSUR using a full data set. The parameter estimates of all the models were significant ($p < 0.05$), and their magnitudes were consistent with biological logics.

Table 5. Parameter estimates of the models (nonlinear error-in-variable models, NEIVM; nonlinear seemingly unrelated regression, NSUR).

Parameters	Model I.4	Model II	TSEM			NSUR		
			Model (6)	Model (7)	Model (8)	Model (6)	Model (7)	Model (8)
α_1	49.7128							
α_2	0.04028							
β_1		0.0768	0.0667	0.0735	0.0859	0.0108	3.2675	0.0794
β_2		2.2550	2.3065	2.2827	2.2280	2.3317	1.7254	2.2435
β_3		0.1266	0.0735	0.0691	0.0721	0.0107	0.0603	0.0737
β_4		1.8635	1.9435	0.0477	1.9545	2.0060	2.5465	1.9387
β_5		0.0737	0.0431	1.8584	0.0406	0.0062	0.5010	0.0409
β_6		1.9386	1.8826	2.2196	1.9064	1.9466	1.7892	1.8961
β_7		0.0421	0.0726	0.0667	0.0555	0.0107	0.0007	0.0449
β_8		1.8861	1.5177	1.5461	1.6099	1.5746	1.6928	1.6776
β_9		0.2465	0.1514	0.1769		0.2096	0.1924	
β_{10}		2.0474	2.1951	2.1359		2.0877	2.1169	
β_{11}		0.1160		1.9600			0.1925	
β_{12}		2.1738		0.0995			2.3012	
β_{13}		0.0613		0.1289			0.3223	
β_{14}		1.5708		1.8295			1.8211	

3.3. Model Evaluation

Table 6 shows the comparisons of the performances of different component models of NEIVM and NSUR with one-step, two-step, and summation (Equations (6)–(8)). The fitting precisions of all the components with one-step were slightly higher than those of TSEM and NSUR. For example, for bark, R^2 with NSUR-one-step was 0.5883, which was 1.94% higher than models with NSUR-two-step. For the nonlinear seemingly unrelated regression, the difference in the fitting effects of all the components with different methods were very small; TSEM also had this effect. The order of the fitting precision of different tree-component biomass models were: protoxylem model < branch model < bark model < foliage model.

Table 6. The performance of the three model systems with two-parameter estimation methods.

Component	Method	R^2	$\bar{\varepsilon}_W$	TRE	RMSE
Protoxylem	TSEM-one-step	0.5585	0.7367	17.3555	19.7769
	TSEM-two-step	0.5571	1.3899	18.1241	19.8083
	TSEM-summation	0.5567	−1.6579	15.9434	19.8157
	NSUR-one-step	0.5598	−0.1139	16.9208	19.7469
	NSUR-two-step	0.5598	−0.1386	16.9182	19.7470
	NSUR-summation	0.5597	−0.1631	16.9260	19.7482
Branch	TSEM-one-step	0.5831	0.2232	13.0848	6.5200
	TSEM-two-step	0.5818	0.4157	13.5562	6.5306
	TSEM-summation	0.5820	−0.4344	12.2372	6.5287
	NSUR-one-step	0.5841	−0.0557	12.7713	6.5124
	NSUR-two-step	0.5843	0.0163	12.7756	6.5111
	NSUR-summation	0.5839	−0.0522	12.7779	6.5137

Table 6. *Cont.*

Component	Method	R^2	$\bar{\varepsilon}_W$	TRE	RMSE
Bark	TSEM-one-step	0.5875	0.1046	12.4149	3.1123
	TSEM-two-step	0.5861	0.1944	12.8460	3.1175
	TSEM-summation	0.5864	−0.1985	11.6462	3.1163
	NSUR-one-step	0.5883	−0.0306	12.1221	3.1089
	NSUR-two-step	0.5710	0.2621	12.7672	3.1736
	NSUR-summation	0.5882	−0.0190	12.1310	3.1096
Foliage	TSEM-one-step	0.6141	0.0445	8.7044	1.5164
	TSEM-two-step	0.6126	0.0829	8.9405	1.5195
	TSEM-summation	0.6131	−0.0693	8.3161	1.5185
	NSUR-one-step	0.6139	−0.0333	8.5344	1.5169
	NSUR-two-step	0.5840	−0.1341	9.2154	1.5746
	NSUR-summation	0.6125	0.0268	8.5872	1.5196
Above-ground	TSEM-one-step	0.5753	−0.2478	14.1597	31.5338
	TSEM-two-step	0.5753	−0.2478	14.1597	31.5338
	TSEM-summation	0.5685	−2.3602	14.0111	30.9364
	NSUR-one-step	0.5753	−0.2478	14.1597	31.5338
	NSUR-two-step	0.5753	−0.2478	14.1597	31.5338
	NSUR-summation	0.5710	−0.2075	14.7572	30.8468

3.4. Reduction of Heteroscedasticity

We tested weight functions $1/\sqrt[3]{f_i(y_i^{(1)}, x_i, \beta_1)}$, $1/\sqrt{f_i(y_i^{(1)}, x_i, \beta_1)}$, $1/f_i(y_i^{(1)}, x_i, \beta_1)$ and $1/f_i(y_i^{(1)}, x_i, \beta_1)^2$ to reduce the heteroscedasticity. Finally, the weight function $1/\sqrt{f_i(y_i^{(1)}, x_i, \beta_1)}$ showed a better performance (Figure 4). This study confirms that the heteroscedasticity of the joint system of equations can be reduced using a weight function, and therefore, we suggest using the equation $1/\sqrt{f_i(y_i^{(1)}, x_i, \beta_1)}$.

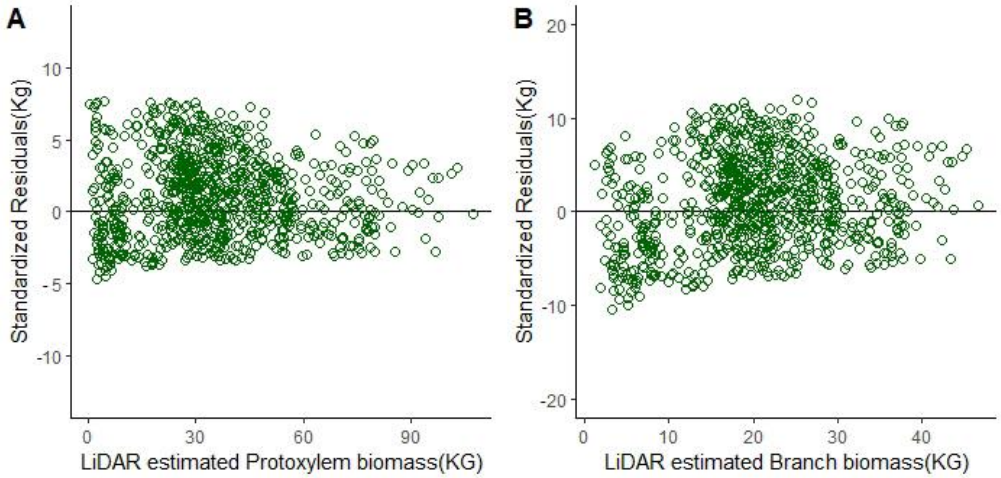

Figure 4. *Cont.*

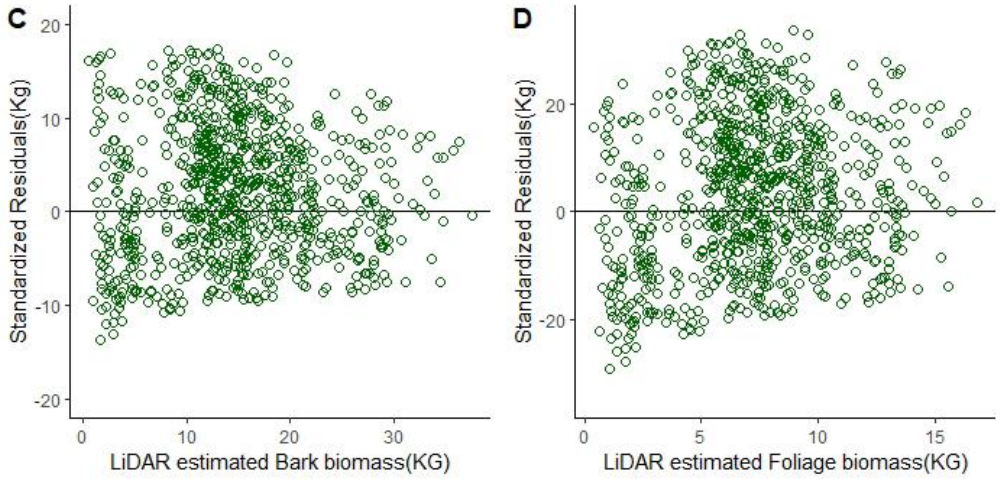

Figure 4. The residuals of the tree-components biomass model with a weight function $1/\sqrt{f_i(y_i^{(1)}, x_i, \beta_1)}$ based on the NSUR-one-step method. (**A**–**D**) represent the residuals of the protoxylem biomass, branch biomass, bark biomass, and foliage biomass, respectively.

4. Discussion

Forests are the mainstays of the terrestrial ecosystem [61]. Precise quantification of forest biomass for the evaluation of ecosystem functions and productivities is necessary. Methods of obtaining forestry data, including biomass, carbon storage, and some other forest survey data that are timely and effective have always been a concern in forest science [62]. In our study, we used error-in-variable modeling to develop an additive model system of tree protoxylem, branch, bark, and foliage with the use of the airborne LiDAR data. A model system not only ensured the compatibility of DBH and different component biomasses, it also ensured the additivity of different component biomasses. In the first step, we built the correlations between the DBH and different component biomasses with the assumptions that the observations of the independent variables would have no measurement error in them, while the observations of the dependent variable would contain measurement errors. Generally, if a measurement error existed in the observed value of the independent variable, the estimation of the model might be largely biased. However, the error-in-variable model could be theoretically unbiased [63], and the findings of Fu et al. [37] also supported this.

In our study, only LiDAR-derived tree height was included in a biomass model system. As an individual, LH had the highest contribution to DBH and was consistent with statistical modeling principles [64]. From a remote sensing perspective, the canopy diameter would be more difficult to measure than LH and CPA because of a complex crown shape [65]. Several studies found a strong relationship between canopy diameter and DBH [66,67]. For example, several researchers [68–70] mentioned that canopy diameter could be measured based on the geometric method of the crown projection area. In our study, both the effects of canopy diameter and crown projection area on the LiDAR-DBH model were evaluated, and it was found that canopy diameter did not significantly contribute to the model improvement; however, the crown projection area had a significant contribution to improving the LiDAR-DBH model. Additionally, the crown projection area had a significant collinearity problem, and that was why we chose to exclude this. The main reasons were: (i) although the CPA could reflect the crown effects, LH had a stronger relationship with DBH, and (ii) adding the CPA diameter into the model would provide a weaker predictability, as this would increase the model complexity; these variables would significantly correlate with each other. Considering all of this, only the LH was selected as a predictor in our biomass model system. This resulted in the two-parameter model, which could enhance the robustness and stability of the models when the model system is embedded into a complete algorithm in the future.

A previous study showed that the measurement error model was more advantageous when DBH had measurement errors [21,25,62]. In practice, the sources of random error largely vary and are not easy to avoid, such as the airborne LiDAR system, due to weather, space, and other factors. In the process of single-tree segmentation, height estimation accuracy is one of the many factors [71]. In our study, we identified the most suitable parameter estimation method of the measurement error model through a rigorous comparison. For NSUR, the one-step method had only a slight advantage over the two-step method (Table 6). The reason was that we let the stem = protoxylem + bark and the crown = branch + foliage, and there were still some errors between the stem and the crown of the biomass model and the aboveground biomass model, which would lead to an increase in model error. However, the two-step method provided an idea for the LiDAR inversion of the tree biomass when the allometric growth equations of the stem and the crown for obtaining different components of biomass were known. For TSEM, the one-step model system form had an advantage over the summation method (Table 6), and it was because the summation method had one more equation than the proportion method, which increased the system complexity, and was subjected to more constraints in the calculation process. For different components, the performances were different. It might be related to the amounts of biomasses of different components, and a model system was constrained to prefer components with smaller biomasses. Overall, the NSUR one-step method was clearly more convenient and practical than TSEM, which needed to be computed in Forstat because the R nlsystemfit (nonlinear equation system estimation) function [72] had a wider range of users.

Generally, the fitting effect of the model should be identical within a reasonable range [73]. However, for different components, the performance of each method may have large variations. This may be due to fitting data, as this study included the age class of *Larix gmelinii* var. principis-rupprechtii. For the whole tree, the order of the biomasses was protoxylem > branch > bark > foliage (Table 1). The biomasses of bark and leaves in the juvenile forest were small but not much different from that of other age classes. However, the small biomass of protoxylem led to irregularity in the protoxylem data structure. Therefore, we suggest the establishment of different model systems as per age groups in practical applications to improve the estimation accuracies of biomasses.

Heteroscedasticity is a problem that must be solved [74], and the solution is to linearize the model or increase the weight function. In contrast, the former method might increase the complexity of the calculation. Thus, it is necessary to select the appropriate weight function. However, a larger or smaller weight function might cause poor heteroscedasticity reduction; this might be because weight function cannot regulate well the weights of residuals. To explore and select the weight function, we found that the effect of heteroscedasticity reduction would be largely related to the size of the data. This provided a scheme and a suggestion for other similar studies to select the weight function while reducing heteroscedasticity.

We developed this a biomass model system not only to ensure the compatibility of DBH and tree-components but also to ensure the additivity of the aboveground biomass and the different components biomass. This would potentially expend the use of LiDAR data for estimating AGB from tree-components to individual tree and then to stand, which does not require the field measurement data; NSUR-one-step appeared to be the best method. Even though the final fitting effect of each model system was not attractive, the best R^2 was 0.61 for components of foliage. This might be mainly due to: (i) the error propagation, in which the LH-DBH had an error of 0.56, and the DBH-components, which had an error of 0.97; and (ii) the uncertainty of the sources of the relationship between DBH and different components biomass [75]. In our study, only the independent variables were considered without error, but the uncertainties might arise from the error of using LiDAR data, the measurement error of variables, the error of using LiDAR data to delineate tree crowns and estimate LH and DBH, and the model parameters estimation error. Overall, if the error sources were identified clearly, a biomass model system could be improved timely and effectively, which will be our main task in the future.

5. Conclusions

Based on the field measurement data and airborne LiDAR data of principis-rupprechtii trees in north China, the error-in-variable biomass model system was developed to ensure that the individual tree-components biomass and DBH were compatible and to ensure the additivity of the components biomass. Three alternative parameter estimation methods and three forms of a model system, TSEM and NSUR with one-step, two-step, and summation, were evaluated. The performance of NSUR-one-step and TSEM-one-step were almost identical. The models and methods we proposed could provide a reliable precision while estimating both DBH and tree-components biomass, based on the airborne LiDAR data. Our compatible biomass and DBH model system, similar to the one developed by a previous study based on LiDAR data [37], required some processed remote sensing data to obtain the DBH of individual trees and the biomasses of tree-components. Our model system was more comprehensive by incorporating the estimation of individual tree-components and ensured their compatibility and additivity. This meant that the forest biomass or the carbon storage information could be obtained without field measurements. Therefore, our methods and models could be applicable to forest management, and the methods could be applied to other tree species as well. It would be more advantageous if we could identify the other sources of errors to improve the prediction accuracy of a compatibility model system.

Author Contributions: Conceptualization, X.C., D.X. and L.F.; methodology, X.C.; software, X.C. and L.F.; validation, X.C., L.F. and Q.C.; formal analysis, X.C., D.X. and Q.C.; investigation, X.C., Q.L., Z.Z. and D.X.; data curation, X.C., Z.Z., D.X. and L.F.; writing—original draft preparation, X.C. and L.F.; writing—review and editing, L.F. and R.P.S.; visualization, L.F. and R.P.S.; supervision, L.F. and R.P.S.; project administration, L.F.; funding acquisition, L.F. All authors have read and agreed to the published version of the manuscript.

Funding: This research was funded by the 14th Five-Year Plan Pioneering Project of High Technology Plan of the National Department of Technology under Grant 2021YFD2200405.

Conflicts of Interest: The authors declare no conflict of interest.

References

1. Song, X.; Zhou, G.; Jiang, H.; Yu, S.; Fu, J.; Li, W.; Wang, W.; Ma, Z.; Peng, C. Carbon Sequestration by Chinese Bamboo Forests and Their Ecological Benefits: Assessment of Potential, Problems, and Future Challenges. *Environ. Rev.* **2011**, *19*, 418–428. [CrossRef]
2. Dube, T.; Mutanga, O. Quantifying the variability and allocation patterns of aboveground carbon stocks across plantation forest types, structural attributes and age in sub-tropical coastal region of KwaZulu Natal, South Africa using remote sensing. *Appl. Geogr.* **2015**, *64*, 55–65. [CrossRef]
3. Mngadi, M.; Odindi, J.; Mutanga, O.; Sibanda, M. Estimating aboveground net primary productivity of reforested trees in an urban landscape using biophysical variables and remotely sensed data. *Sci. Total Environ.* **2021**, *802*, 149958. [CrossRef] [PubMed]
4. Diamantopoulou, M.J. Artificial Neural Networks as an Alternative Tool in Pine Bark Volume Estimation. *Comput. Electron. Agric.* **2005**, *48*, 235–244. [CrossRef]
5. Diamantopoulou, M.J.; Özçelik, R.; Yavuz, H. Tree-Bark Volume Prediction via Machine Learning: A Case Study Based on Black Alder's Tree-Bark Production. *Comput. Electron. Agric.* **2018**, *151*, 431–440. [CrossRef]
6. Piégay, H.; Pautou, G.; Ruffinoni, C. *Les Forêts Riveraines Des Cours D'eau: Écologie, Fonctions et Gestion*; IDF: Melbourne, Australia, 2003.
7. Claessens, H.; Oosterbaan, A.; Savill, P.; Rondeux, J. Review of the Characteristics of Black Alder (*Alnus glutinosa* (L.) Gaertn.) and Their Implications for Silvicultural Practices. *For. Int. J. For. Res.* **2010**, *83*, 163–175. Available online: https://academic.oup.com/forestry/article/83/2/163/519324?login=false (accessed on 22 February 2023). [CrossRef]
8. Nelson, R.; Krabill, W.; MacLean, G. Determining Forest Canopy Characteristics Using Airborne Laser Data. *Remote Sens. Environ.* **1984**, *15*, 201–212. [CrossRef]
9. Nelson, R.; Krabill, W.; Tonelli, J. Estimating Forest Biomass and Volume Using Airborne Laser Data. *Remote Sens. Environ.* **1988**, *24*, 247–267. [CrossRef]
10. Maclean, G.A.; Krabill, W.B. Gross-Merchantable Timber Volume Estimation Using an Airborne Lidar System. *Can. J. Remote Sens.* **1986**, *12*, 7–18. [CrossRef]
11. Næsset, E. Determination of Mean Tree Height of Forest Stands Using Airborne Laser Scanner Data. *ISPRS J. Photogramm. Remote Sens.* **1997**, *52*, 49–56. [CrossRef]

12. Nelson, R.; Oderwald, R.; Gregoire, T.G. Separating the Ground and Airborne Laser Sampling Phases to Estimate Tropical Forest Basal Area, Volume, and Biomass. *Remote Sens. Environ.* **1997**, *60*, 311–326. [CrossRef]
13. Maltamo, M.; Eerikäinen, K.; Pitkänen, J.; Hyyppä, J.; Vehmas, M. Estimation of Timber Volume and Stem Density Based on Scanning Laser Altimetry and Expected Tree Size Distribution Functions. *Remote Sens. Environ.* **2004**, *90*, 319–330. [CrossRef]
14. Popescu, S.C. Estimating Biomass of Individual Pine Trees Using Airborne Lidar. *Biomass Bioenergy* **2007**, *31*, 646–655. [CrossRef]
15. Pang, Y.; Li, Z.-Y. Inversion of biomass components of the temperate forest using airborne Lidar technology in Xiaoxing'an Mountains, Northeastern of China: Inversion of biomass components of the temperate forest using airborne Lidar technology in Xiaoxing'an Mountains, Northeastern of China. *Chin. J. Plant Ecol.* **2013**, *36*, 1095–1105. [CrossRef]
16. Hudak, A.T.; Strand, E.K.; Vierling, L.A.; Byrne, J.C.; Eitel, J.U.H.; Martinuzzi, S.; Falkowski, M.J. Quantifying Aboveground Forest Carbon Pools and Fluxes from Repeat LiDAR Surveys. *Remote Sens. Environ.* **2012**, *123*, 25–40. [CrossRef]
17. García, M.; Riaño, D.; Chuvieco, E.; Danson, F.M. Estimating Biomass Carbon Stocks for a Mediterranean Forest in Central Spain Using LiDAR Height and Intensity Data. *Remote Sens. Environ.* **2010**, *114*, 816–830. [CrossRef]
18. Singh, K.K.; Chen, G.; Vogler, J.B.; Meentemeyer, R.K. When Big Data Are Too Much: Effects of LiDAR Returns and Point Density on Estimation of Forest Biomass. *IEEE J. Sel. Top. Appl. Earth Obs. Remote Sens.* **2016**, *9*, 3210–3218. [CrossRef]
19. Wang, M.; Liu, Q.; Fu, L.; Wang, G.; Zhang, X. Airborne LIDAR-Derived Aboveground Biomass Estimates Using a Hierarchical Bayesian Approach. *Remote Sens.* **2019**, *11*, 1050. [CrossRef]
20. Ma, K.; Chen, Z.; Fu, L.; Tian, W.; Jiang, F.; Yi, J.; Du, Z.; Sun, H. Performance and Sensitivity of Individual Tree Segmentation Methods for UAV-LiDAR in Multiple Forest Types. *Remote Sens.* **2022**, *14*, 298. [CrossRef]
21. Evaluation of Nonlinear Equations for Predicting Diameter from Tree Height. Available online: https://cdnsciencepub.com/doi/10.1139/x2012-019 (accessed on 22 February 2023).
22. Gleason, C.J.; Im, J. Forest Biomass Estimation from Airborne LiDAR Data Using Machine Learning Approaches. *Remote Sens. Environ.* **2012**, *125*, 80–91. [CrossRef]
23. Broadbent, E.N.; Asner, G.P.; Peña-Claros, M.; Palace, M.; Soriano, M. Spatial Partitioning of Biomass and Diversity in a Lowland Bolivian Forest: Linking Field and Remote Sensing Measurements. *For. Ecol. Manag.* **2008**, *255*, 2602–2616. [CrossRef]
24. Heurich, M. Automatic Recognition and Measurement of Single Trees Based on Data from Airborne Laser Scanning over the Richly Structured Natural Forests of the Bavarian Forest National Park. *For. Ecol. Manag.* **2008**, *255*, 2416–2433. [CrossRef]
25. Zhang, W.; Ke, Y.; Quackenbush, L.J.; Zhang, L. Using Error-in-Variable Regression to Predict Tree Diameter and Crown Width from Remotely Sensed Imagery. *Can. J. For. Res.* **2010**, *40*, 1095–1108. [CrossRef]
26. Ene, L.T.; Næsset, E.; Gobakken, T.; Gregoire, T.G.; Ståhl, G.; Holm, S. A Simulation Approach for Accuracy Assessment of Two-Phase Post-Stratified Estimation in Large-Area LiDAR Biomass Surveys. *Remote Sens. Environ.* **2013**, *133*, 210–224. [CrossRef]
27. Rencher, A.C.; Schaalje, G.B. *Linear Models in Statistics*, 2nd ed.; Wiley: New York, NY, USA, 2008.
28. *Measurement Error Models; Wiley Series in Probability and Statistics*; John Wiley & Sons, Inc.: Hoboken, NJ, USA, 1987. Available online: https://onlinelibrary.wiley.com/doi/book/10.1002/9780470316665 (accessed on 22 February 2023).
29. Verwijst, T.; Telenius, B. Biomass Estimation Procedures in Short Rotation Forestry. *For. Ecol. Manag.* **1999**, *121*, 137–146. [CrossRef]
30. Zellner, A. An Efficient Method of Estimating Seemingly Unrelated Regressions and Tests for Aggregation Bias. *J. Am. Stat. Assoc.* **1962**, *57*, 348–368. Available online: https://www.tandfonline.com/doi/abs/10.1080/01621459.1962.10480664 (accessed on 22 February 2023). [CrossRef]
31. Bi, H.; Birk, E.; Turner, J.; Lambert, M.; Jurskis, V. Converting stem volume to biomass with additivity, bias corrections and confidence bands for two Australian tree species. *N. Zealand J. For. Sci.* **2001**, *31*, 298–319.
32. Bi, H.; Turner, J.; Lambert, M.J. Additive Biomass Equations for Native Eucalypt Forest Trees of Temperate Australia. *Trees* **2004**, *18*, 467–479. Available online: https://link.springer.com/article/10.1007/s00468-004-0333-z (accessed on 22 February 2023). [CrossRef]
33. Bi, H.; Long, Y.; Turner, J.; Lei, Y.; Snowdon, P.; Li, Y.; Harper, R.; Zerihun, A.; Ximenes, F. Additive Prediction of Aboveground Biomass for Pinus Radiata (D. Don) Plantations. *For. Ecol. Manag.* **2010**, *259*, 2301–2314. [CrossRef]
34. Fu, L.; Lei, Y.; Wang, G.; Bi, H.; Tang, S.; Song, X. Comparison of Seemingly Unrelated Regressions with Error-in-Variable Models for Developing a System of Nonlinear Additive Biomass Equations. *Trees* **2016**, *30*, 839–857. [CrossRef]
35. Parresol, B.R. Assessing Tree and Stand Biomass: A Review with Examples and Critical Comparisons. *For. Sci.* **1999**, *45*, 573–593.
36. Lei, X.; Zhang, H.; Bi, H. Additive Aboveground Biomass Equations for Major Tree Species in Over-Logged Forest Region in Northeast China. In Proceedings of the 2012 IEEE 4th International Symposium on Plant Growth Modeling, Simulation, Visualization and Applications, Shanghai, China, 31 October–3 November 2012; pp. 220–223.
37. Fu, L.; Liu, Q.; Sun, H.; Wang, Q.; Li, Z.; Chen, E.; Pang, Y.; Song, X.; Wang, G. Development of a System of Compatible Individual Tree Diameter and Aboveground Biomass Prediction Models Using Error-In-Variable Regression and Airborne LiDAR Data. *Remote Sens.* **2018**, *10*, 325. [CrossRef]
38. Kangas, A.S. Effect of Errors-in-Variables on Coefficients of a Growth Model and on Prediction of Growth. *For. Ecol. Manag.* **1998**, *102*, 203–212. [CrossRef]
39. A Study on Impact of Measurement Error on Whole Stand Model. Available online: http://www.linyekexue.net/EN/10.11707/j.1001-7488.20050629 (accessed on 22 February 2023).
40. Moore, J.R. Allometric Equations to Predict the Total Above-Ground Biomass of Radiata Pine Trees. *Ann. For. Sci.* **2010**, *67*, 806. [CrossRef]

41. *Measurement Error: Models, Methods, and Applications*, 1st ed.; CRC Press: Boca Raton, FL, USA, 2010. Available online: https://www.routledge.com/Measurement-Error-Models-Methods-and-Applications/Buonaccorsi/p/book/9781032477688 (accessed on 22 February 2023).
42. Koch, B.; Heyder, U.; Weinacker, H. Detection of Individual Tree Crowns in Airborne Lidar Data. *Photogramm. Eng. Remote Sens.* **2006**, *72*, 357–363. [CrossRef]
43. Parent, J.R.; Volin, J.C. Assessing the Potential for Leaf-off LiDAR Data to Model Canopy Closure in Temperate Deciduous Forests. *ISPRS J. Photogramm. Remote Sens.* **2014**, *95*, 134–145. [CrossRef]
44. Chen, Q.; Baldocchi, D.; Gong, P.; Kelly, M. Isolating Individual Trees in a Savanna Woodland Using Small Footprint Lidar Data. *Photogramm. Eng. Remote Sens.* **2006**, *72*, 923–932. [CrossRef]
45. MA, K.; Xiong, Y.; Jiang, F.; Chen, S.; Sun, H. A Novel Vegetation Point Cloud Density Tree-Segmentation Model for Overlapping Crowns Using UAV LiDAR. *Remote Sens.* **2021**, *13*, 1442. [CrossRef]
46. Liu, J.; Shen, J.; Zhao, R.; Xu, S. Extraction of Individual Tree Crowns from Airborne LiDAR Data in Human Settlements. *Math. Comput. Model.* **2013**, *58*, 524–535. [CrossRef]
47. Lopatin, J.; Dolos, K.; Hernández, H.J.; Galleguillos, M.; Fassnacht, F.E. Comparing Generalized Linear Models and Random Forest to Model Vascular Plant Species Richness Using LiDAR Data in a Natural Forest in Central Chile. *Remote Sens. Environ.* **2016**, *173*, 200–210. [CrossRef]
48. Fu, X.; Jiang, D.; Wang, L.; Gao, X.; Qian, D. Study on biomass of Larixprincipis rupprechtiiin Saihanba Mechanized Forestry Centre. *Hebei J. For. Orchard. Res.* **2015**, *30*, 113–116.
49. Venables, W.N.; Ripley, B.D. Graphics. In *Modern Applied Statistics with S-PLUS*; Venables, W.N., Ripley, B.D., Eds.; Statistics and Computing; Springer: New York, NY, USA, 1999; pp. 53–92, ISBN 978-1-4757-3121-7.
50. Yang, Y.; Huang, S. Comparison of Different Methods for Fitting Nonlinear Mixed Forest Models and for Making Predictions. *Can. J. For. Res.* **2011**, *41*, 1671–1686. [CrossRef]
51. Weisheng, Z.; Shouzheng, T. Using Measurement Error Modeling Method to Establish Compatible Single-Tree Biomass Equations System. *For. Res. Beijing* **2010**, *23*, 797–803.
52. Tang, S.Z.; Li, Y. An algorithm for estimating multivariatenon-linear error-in-measure models. *J. Biomath.* **1996**, *11*, 23–27. (In Chinese)
53. Zeng, W.; Tang, S. Modeling Compatible Single-Tree Aboveground Biomass Equations for Masson Pine (*Pinus massoniana*) in Southern China. *J. For. Res.* **2012**, *23*, 593–598. [CrossRef]
54. Tang, S.; Li, Y.; Wang, Y. Simultaneous Equations, Error-in-Variable Models, and Model Integration in Systems Ecology. *Ecol. Model.* **2001**, *142*, 285–294. [CrossRef]
55. Tang, S.; Lang, K.J.; Li, H.K. *Statistics and Computation of Biomathematical Models (ForStat Course)*; Science Press: Beijing, China, 2008. (In Chinese)
56. Kozak, A.; Kozak, R. Does Cross Validation Provide Additional Information in the Evaluation of Regression Models? *Can. J. For. Res.* **2003**, *33*, 976–987. [CrossRef]
57. Zeng, W.; Tang, S. Goodness Evaluation and Precision Analysis of Tree Biomass Equations. *Sci. Silvae Sin.* **2011**, *47*, 106–113.
58. Berk, K.N. Validating Regression Procedures With New Data. *Technometrics* **1984**, *26*, 331–338. [CrossRef]
59. Rao, C.R.; Wu, Y. Linear Model Selection by Cross-Validation. *J. Stat. Plan. Inference* **2005**, *128*, 231–240. [CrossRef]
60. Zeng, W.; Luo, Q.; He, D. Research on weighting regression and modeling. *Sci. Silvae Sin.* **1999**, *35*, 5–11.
61. Field, C.; Raupach, M. *The Global Carbon Cycle: Integrating Humans, Climate and the Natural World*; Island Press: Washington, DC, USA, 2004.
62. He, Q.; Chen, E.; An, R.; Li, Y. Above-Ground Biomass and Biomass Components Estimation Using LiDAR Data in a Coniferous Forest. *Forests* **2013**, *4*, 984–1002. [CrossRef]
63. Fernandes, R.; Leblanc, S.G. Parametric (modified least squares) and non-parametric (Thei-Sen) linear regression for predicting biophysical parameter in the presence of measurement errors. *Remote Sens. Environ.* **2005**, *95*, 303–316. [CrossRef]
64. Antonova, S.; Thiel, C.; Höfle, B.; Anders, K.; Helm, V.; Zwieback, S.; Marx, S.; Boike, J. Estimating Tree Height from TanDEM-X Data at the Northwestern Canadian Treeline. *Remote Sens. Environ.* **2019**, *231*, 111251. [CrossRef]
65. Verma, N.K.; Lamb, D.W.; Reid, N.; Wilson, B. An Allometric Model for Estimating DBH of Isolated and Clustered Eucalyptus Trees from Measurements of Crown Projection Area. *For. Ecol. Manag.* **2014**, *326*, 125–132. [CrossRef]
66. Hall, R.J.; Morton, R.T.; Nesby, R.N. A Comparison of Existing Models for DBH Estimation from Large-Scale Photos. *For. Chron.* **1989**, *65*, 114–120. Available online: https://pubs.cif-ifc.org/doi/10.5558/tfc65114-2 (accessed on 23 February 2023). [CrossRef]
67. Gering, L.R.; May, D.M. The Relationship of Diameter at Breast Height and Crown Diameter for Four Species Groups in Hardin County, Tennessee. *S. J. Appl. For.* **1995**, *19*, 177–181. [CrossRef]
68. Fleck, S.; Mölder, I.; Jacob, M.; Gebauer, T.; Jungkunst, H.F.; Leuschner, C. Comparison of Conventional Eight-Point Crown Projections with LIDAR-Based Virtual Crown Projections in a Temperate Old-Growth Forest. *Ann. For. Sci.* **2011**, *68*, 1173–1185. [CrossRef]
69. Nelson, R. Modeling Forest Canopy Heights: The Effects of Canopy Shape. *Remote Sens. Environ.* **1997**, *60*, 327–334. [CrossRef]
70. Grote, R. Estimation of Crown Radii and Crown Projection Area from Stem Size and Tree Position. *Ann. For. Sci.* **2003**, *60*, 393–402. [CrossRef]

71. Tang, S.Z.; Li, Y.; Fu, L.Y. *Statistical Foundation for Biomathematical Models*, 2nd ed.; Higher Education Press: Beijing, China, 2015; p. 435, ISBN 978-7-04-042303-7.
72. Henningsen, A.; Hamann, J.D. Systemfit: A Package for Estimating Systems of Simultaneous Equations in R. *J. Stat. Softw.* **2008**, *23*, 1–40. [CrossRef]
73. Zhang, M.; Lin, H.; Zeng, S.; Li, J.; Shi, J.; Wang, G. Impacts of Plot Location Errors on Accuracy of Mapping and Scaling Up Aboveground Forest Carbon Using Sample Plot and Landsat TM Data. *IEEE Geosci. Remote Sens. Lett.* **2013**, *10*, 1483–1487. Available online: https://ieeexplore.ieee.org/document/6525401 (accessed on 23 February 2023). [CrossRef]
74. Yang, J.; Xiao, S. The influence of Heteroscedasticity on the Establishment of Biomass Model. *For. Eng.* **2014**, *30*, 25–28.
75. Wang, G.; Zhang, M.; Gertner, G.Z.; Oyana, T.; McRoberts, R.E.; Ge, H. Uncertainties of Mapping Aboveground Forest Carbon Due to Plot Locations Using National Forest Inventory Plot and Remotely Sensed Data. *Scand. J. For. Res.* **2011**, *26*, 360–373. [CrossRef]